Flexibility in a Drug Transport Accessory Protein: Molecular Dynamics Simulations of MexA

Loredana Vaccaro,* Vassilis Koronakis,† and Mark S. P. Sansom*
*Department of Biochemistry, University of Oxford, Oxford OX1 3QU, United Kingdom; and †Department of Pathology, University of Cambridge, Cambridge CB2 1QP, United Kingdom

ABSTRACT Drug resistance in Gram-negative bacteria may be conferred via efflux through a tripartite complex of an inner membrane pump, an outer membrane pore, and a periplasmic adaptor protein. These are AcrB, TolC, and AcrA, respectively, in *Escherichia coli*. In *Pseudomonas aerugonisa*, their homologs are MexB, OprM, and MexA. Defining the interdomain dynamics of the adaptor protein is essential to understanding the mechanism of complex formation. Extended (25 ns) molecular dynamics simulations of MexA have been performed to determine such interdomain dynamics. Analysis of conformational drift demonstrates substantial motions of the three domains of MexA relative to one another. Principal components analysis reveals a hinge-bending motion and rotation of the α-helical hairpin relative to the other domains to be the two dominant motions. These two motions provide an element of considerable flexibility which is likely to be exploited in the adaptor function of MexA.

INTRODUCTION

Drug resistance in bacteria is conferred by inner membrane (IM) efflux proteins or pumps (1–3). These pumps can expel a wide range of antibiotics, resulting in multi-drug resistance and complicating the development of novel therapies. In Gram-negative bacteria a number of these efflux pumps recruit an outer membrane (OM) channel plus a periplasmic protein and assemble into a tripartite drug transport complex (3–5). This complex spans the entire periplasmic region, forming to a long molecular 'tunnel' for drugs, which are thus directly extruded from the cell without release into the periplasm (6,7).

AcrB is an IM efflux pump from *Escherichia coli*. The solute specificity of AcrB is quite broad, as the pump is able to extrude cationic, anionic, and neutral substrates. AcrB is a proton antiporter. It interacts with the OM tunnel protein TolC (8). The interactions between AcrB and TolC are mediated by a third accessory protein, AcrA, which is located in the periplasm. All three components are required for drug transport across the two membranes (i.e., the IM and OM; Fig. 1 *A*). In *Pseudomonas aeruginosa*, the corresponding proteins and their percentage sequence identities to their *E. coli* homologs are MexB (homologous to AcrB, 69% identity), OprM (homologous to TolC, 19% identity), and the periplasmic protein MexA (homologous to AcrA, 57% identity).

The x-ray crystal structure of AcrB has been solved (9) at 3.5-Å resolution. AcrB is a trimer, with each monomer containing 1049 amino acids. The monomer is made up of two main domains, a periplasmic, extramembranous headpiece and a transmembrane (TM) region. These are ~70-Å and ~50-Å thick, respectively. The top of the periplasmic domain of AcrB has a diameter of ~30 Å, similar to the internal diameter (~35 Å) of the lower part of TolC (8). TolC is a trimeric protein, composed of two domains. An ~100-Å-long α-helical barrel spans the periplasm, and a 12-stranded β-barrel spans the OM. A similar structure has been observed recently for OprM, a TolC homolog from *P. aeruginosa* (10) and for the *Vibrio cholerae* homolog VceC (11).

To form a continuous transport system across the IM, periplasm, and OM, the IM and OM components of the efflux pump are connected by a periplasmic adaptor protein. The structure of the AcrA homolog from *P. aeruginosa*, MexA, has been determined (12,13). More recently, the structure of the *E. coli* protein AcrA has become available and shows a close conservation of the structural elements found in MexA (14). In Fig. 1 *B* we show the three domains of MexA: an α-helical hairpin; a β-sheet domain (formed by a lipoyl and a β-barrel subdomain); and a small C-terminal α-helix. In this structure the C-terminus is in close proximity to the N-terminus. This excludes a membrane fusion model (15,16) for this adaptor protein, as it would require a reversible disruption of three stable domains. From the crystal structure, an interaction between the α-helical hairpin of MexA and the coiled coil periplasmic domain of OprM might be proposed. Although the MexA monomers pack together in the crystallographic asymmetric unit such that the hairpin loops of the two arcs are arranged head-to-head, this arrangement is not likely to exist in vivo. Indeed, the adaptor protein is anchored to the IM by a single TM helix or by a fatty acid N-terminus. In this orientation the α-helical hairpin would extend in the periplasm, leading to a possible interaction with the base of the OM protein. As shown by direct cross-linking and isothermal calorimetry (17), AcrA and TolC contact each other. It is reasonable to speculate that such a protein-protein contact is mediated by the α-helices of

Submitted December 20, 2005, and accepted for publication April 18, 2006.
Address reprint requests to Mark S. P. Sansom, Tel.: 44-1865-275371; Fax: 44-1865-275273; E-mail: mark.sansom@bioch.ox.ac.uk.

0006-3495/06/07/558/07 $2.00
doi: 10.1529/biophysj.105.080010

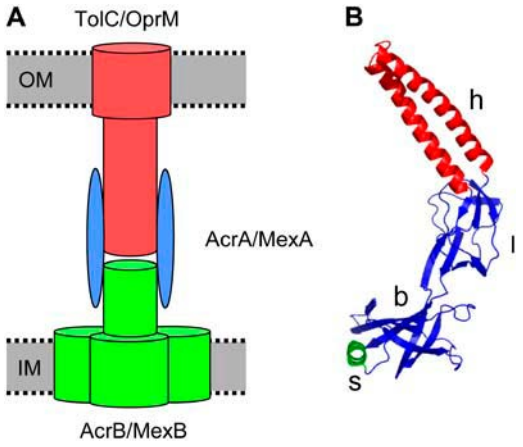

FIGURE 1 (*A*) Schematic diagram of the proposed transport complex formed by AcrB/MexB (*green*), AcrA/MexA (*blue*), and TolC/OprM (*red*) with the IM and the OM shown as gray bands. (*B*) The x-ray crystal structure of the MexA monomer from *Pseudomonas aeruginosa*. Three major domains can be distinguished: an α-helical hairpin (*h*, *red*); a β-domain (*blue*) made up of a lipoyl (*l*) and a β-barrel (*b*) subdomain; and a short α-helix (s, *green*).

the two proteins. Furthermore, the (α + β)-domain of the adaptor would be located proximal to he IM protein (AcrB/MexB). Biochemical and genetic data suggest that the C-terminal domain of AcrA/MexA contacts the IM component, AcrB/MexB (17–19). Nevertheless, despite a general acceptance of the orientation of MexA within the periplasm, a number of different models have been proposed for the interaction of it with the other two proteins (12,13,20). A threefold symmetric ring of MexA monomers is generally favored, although the exact number of monomers remains to be defined. In the crystal structures of AcrB and TolC (and of OprM) the pore running through the center of each protein is closed (at the periplasmic mouth of the pore in the case of TolC and OprM). It is possible that the interaction between TolC and the adaptor protein (i.e., AcrA/MexA) leads to opening of the exit pore.

As suggested by Fernandez-Recio et al. (20), a structural adjustment by the periplasmic adaptor protein seems to be required to engage both the bottom part of TolC and the top region of AcrB. Molecular dynamics (MD) simulations provide one way to explore conformational flexibility of proteins (21). Alternative approaches include, e.g., normal mode analysis (22) (which shares a common force field with MD simulations). In this work we use three MD simulations of duration $\geq$20 ns combined with principal components analysis (PCA) to describe the conformational dynamics of MexA. The major motions observed are the hinge bending of the two domains and the rotation of the β-barrel domain. These can be related with the role of MexA as a flexible molecular adaptor between the OM and IM proteins during the assembly and opening of functional pores across the two-membrane system.

METHODS

The 3.0-Å resolution x-ray structure of MexA (Protein Data Bank code 1T5E) was used as a starting structure. A single monomer was solvated with SPC water. The protonation states of the amino acids were based on pK_A calculations performed using WHATIF (23), setting the pH at 7. Na^+ and Cl^- ions were added in numbers equivalent to a ~0.1-M solution. The total simulation system was therefore ~166,000 atoms. The simulation was performed using GROMACS (www.gromacs.org) (24). The LINCS algorithm (25) was used to constrain all bond lengths. A cutoff of 1.0 nm for Lennard-Jones interactions was used, and the particle mesh Ewald method (26,27) was employed to calculate longer-range electrostatic contributions on a grid with a 0.12-nm spacing and a cutoff of 1.0 nm. The simulation was conducted at constant temperature (300 K), coupling each component separately to a temperature bath with a coupling constant τ_T of 0.1 ps using the Berendsen coupling method (28). A constant pressure of 1 bar has been applied in all the three directions, with a coupling constant of 1.0 ps. The time step used was 2 fs, with coordinates stored every 2 ps. Three simulations were performed, with different random seeds: MD1 was 25 ns in duration, whereas simulations MD2 and MD3 were each of duration 20 ns.

Before running each simulation, an energy minimization was performed. The first 0.5 ns of simulation were performed imposing positional restraints on the non-H atoms of the protein, applying a force constant of 1000 kJ mol^{-1} nm^{-1}. The positional restraints were then released and 20–25-ns production runs were obtained and analyzed.

Analysis programs from GROMACS were used. Secondary structure analysis used DSSP (29). The Dynamite server (www.biop.ox.ac.uk/dynamite (30)) was used to aid PCA of the MD trajectory. Visualization used visual molecular dynamics (31).

RESULTS

Stability of the simulation and dynamics of MexA

As a first check of the stability of simulation MD1, the root mean-square deviation (RMSD) of MexA from its initial conformation may be determined. To this end the RMSD of the protein Cα atoms has been evaluated (Fig. 2 *A*). In the first 18 ns of the simulation a quasiperiodic behavior of the RMSD is observed, followed by a more monotonic increase after 18 ns. Despite a relatively high final Cα RMSD (~0.6 nm), the fold of the protein remained intact. A similar behavior is seen in simulations MD2 and MD3, with a quasiperiodic behavior of the RMSD being seen in both cases.

From visualization and from analysis of the secondary structure as a function of time, it was evident that no dramatic changes in fold occurred. Instead, it appeared that the relatively large RMSD was due to interdomain motions. Subsequently, to define the largest contribution to the RMSD from the different domains of the protein, the RMSDs of the single domains with respect to their starting coordinates were also determined (Fig. 2 *B*). From this analysis it appeared that the largest deviations from the initial conformation were due to the β-barrel domain during the whole simulation and to the α-helical hairpin during the first 5 ns of the simulation. Nevertheless, there is no dramatic increase of any of these plots. Thus the individual domains did not undergo any substantial conformation drift, indicating that high overall RMSD must reflect interdomains motions.

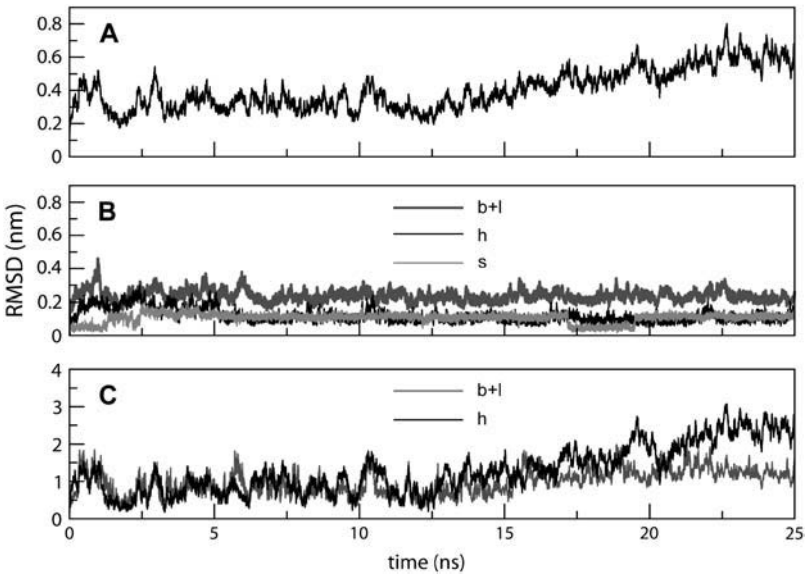

FIGURE 2 RMSD of the Cα atoms from their initial coordinates as a function of time, for simulation MD1. (*A*) RMSD for the whole protein. (*B*) RMSDs for the different domains (as defined in Fig. 1): the α-helical hairpin (*h*, *black line*), the β-domain (*b* + *l*, *thick dark gray line*), and the short α-helix (*s*, *thin pale gray line*). (*C*) RMSD for the Cα atoms of the β-domain (*b* + *l*, *dark gray line*) calculated while fitting onto the starting Cα coordinates of the α-helical hairpin (see text for details), and the RMSD for the α-helical hairpin (*h*, *black line*) calculated while fitting onto the starting Cα coordinates of the β-domain.

To explore the relative motions of different domains, the RMSD of the β-sheet domain with respect to the starting structure with fitting of successive simulations frames on the α-hairpin domain and vice versa have been analyzed. The results are shown in Fig. 2 *C*. By calculating the RMSD of one domain with respect to the starting position of the other domain, we focus on the motion of the analyzed domain, keeping the other fixed. From Fig. 2 *C* it can be seen that, for the first 18 ns of simulation, the Cα RMSD of the α-hairpin with respect to the β-sheet has a similar magnitude and temporal profile to the Cα RMSD of the β-sheet with respect to the α-hairpin. This is thought to be a consequence of a concerted motion of the two domains in which neither one dominates the other. Furthermore, these two RMSDs correspond with that for the protein as a whole (Fig. 2 *A*). This indicates that this concerted motion of the two domains is the major contribution to the global motion of the protein during the first part of the simulation. After 18 ns, the RMSD of the hairpin shows an increase as well as the total RMSD. This result is in agreement with a dominant motion of the hairpin with respect to the rest of the protein responsible for the increase in the total RMSD.

Principal components analysis

A common approach in the identification of the major motions of a protein is the use of PCA (32,33). This general method is widely used to reduce the dimensionality of a complex data set and so can be applied to decompose a complex motion of proteins into a few principal motions, each of which is characterized by an eigenvector and an eigenvalue. The eigenvalue for a given motion represents the contribution of the corresponding eigenvector to the global motion of the protein.

PCA of the MexA simulation reveals that the first 10 eigenvectors account for 92% of the global motion in simulation MD1 and that the first eigenvector corresponds to 53% of the total motion and the second to a further 20% (Fig. 3). The comparable figures are 52% and 20% for MD2, and 37% and 23% for MD3. Thus, a first approximation is provided by restricting our analysis to the first two eigenvectors, with this providing a reliable description of the dynamics of the protein. Visualization of the eigenvectors (via Dynamite) generates a 'porcupine' plot (34). In this representation, each Cα atom is linked to a cone which points in the direction of motion described by the eigenvector for that atom. The length of the cone is proportional to the amplitude of the corresponding motion. From such analysis applied to all three simulations (Fig. 4) it can be seen that in MD1 and MD3 the first principal motion is a rotation of the β-sheet domain

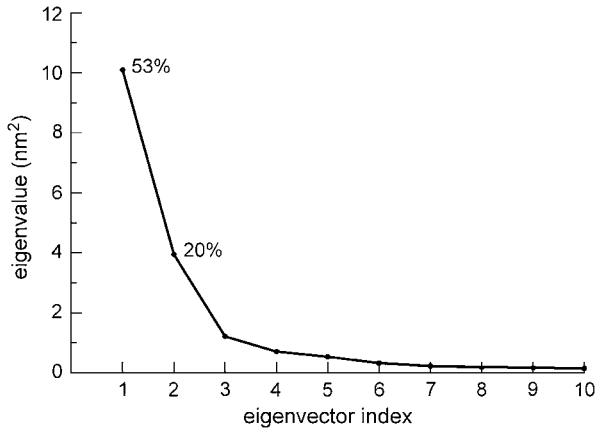

FIGURE 3 Eigenvalue spectra of the diagonalized covariance matrix, for simulation MD1. The first eigenvector contributes 53% to the total motion of the protein, whereas the second eigenvector contributes 20%.

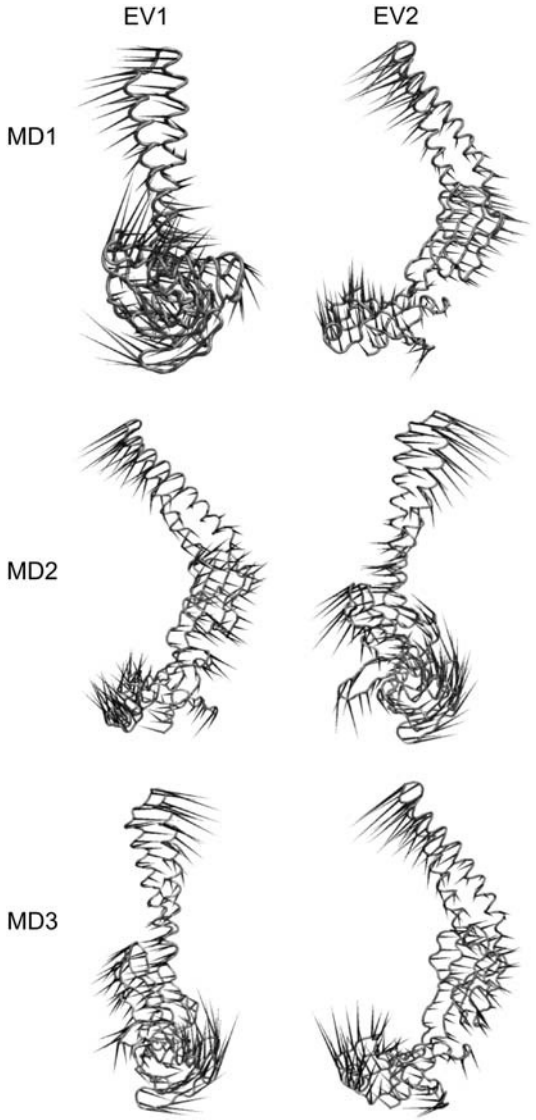

FIGURE 4 Images of the motions corresponding to the first two eigenvectors for simulations MD1, MD2, and MD3. Each Cα atom has a cone attached pointing in the direction of motion described in the eigenvector for that atom. Thus, in simulations MD1, the first eigenvector (*EV1*) corresponds to a rotation of the small α-helix at the end of the β-barrel subdomain; and the second eigenvector (*EV2*) corresponds to a hinge-bending motion between the α-helical hairpin and the β-domain. The same pattern is seen in simulation MD3, whereas in MD2 the hinge-bending motion is EV1 and the rotation is EV2.

and consequent bending of the helical hairpin, whereas the second eigenvector is a hinge bending of the two domains. In MD2 the first eigenvector corresponds to hinge bending, and the second eigenvector to rotation.

To better understand the behavior of MexA during the 25 ns of simulation MD1, a projection of the trajectory onto the first two eigenvectors was analyzed (Fig. 5). Starting from a middle position (close to the projection of the starting coordinates of MexA onto the two eigenvectors), the protein first samples a region on the left of the plot (in *red*), and after 15 ns, it goes to a different region of the plane to the right (highlighted in *blue*) by passing through conformations similar to the starting structure. Thus, the protein is sampling different conformational spaces during the simulation. This can be viewed as a passage from one energy minimum to another, starting from a saddle point, the x-ray structure, and crossing it again during the simulation. In the first minimum, the protein undergoes mostly a hinge-bending motion of the two main domains whereas in the second, rotation of the α-helical hairpin is observed. This is revealed by the snapshots of the average structures extracted along the simulation trajectory (Fig. 5, *A–C*).

It is interesting to point out that if one analyzes a shorter trajectory (the initial 15 ns) the same two eigenvectors were observed, but inverted, i.e., the hinge bending was the first eigenvector and the rotation the second one. Thus, a shorter simulation did not as completely sample the conformational space but did reveal the overall pattern of flexibility of the protein.

These movements provide considerable flexibility within MexA, enabling it to dynamically bridge the IM and OM proteins of the drug efflux complex (MexB and OprM, respectively). Both the hinge bending and the rotation of the domains thus may be related to the biological activity of MexA, helping it to link together the IM and the OM proteins.

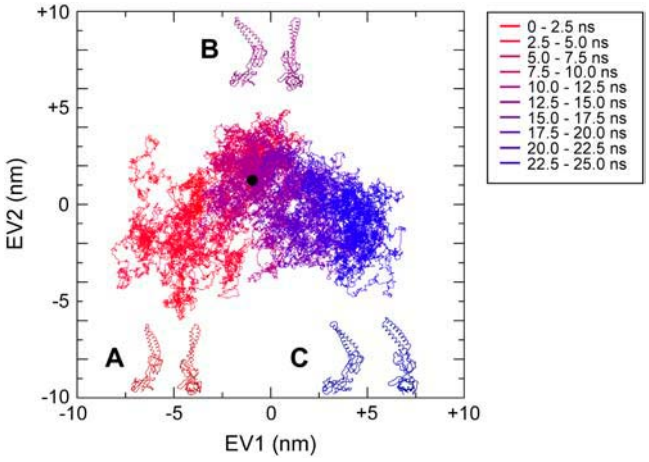

FIGURE 5 Projections of the trajectory of the MexA simulation onto the first (*EV1*) and second (*EV2*) eigenvectors. A gradient of colors from red to blue is used to track the protein over the 25 ns of simulation. The black circle indicates the projection of the starting structure onto the first and second eigenvectors. Two distinct conformational spaces are sampled during the simulation; the left-hand section of the plot (mostly in *red*) corresponds to hinge-bending of the two principal domains, whereas the right-hand section (mostly in *blue*) corresponds to rotation of the hairpin with respect to the β-strands. In red (*A*), we show the average structure over the first 5 ns, in purple (*B*) the average between 5 and 10 ns, and in blue (*C*) the average over the last 5 ns. In the first structure, an enlargement of the angle between the two domains is observed, corresponding to the hinge-bending motion, whereas the major difference between the blue structure and the x-ray structure lies in the bending of the hairpin.

The flexibility of a protein is also often revealed by looking at the root mean-square fluctuation (RMSF) of each residue from its time-averaged position. (The average was calculated for the whole 25 ns of simulation MD1.) In Fig. 6 we show the Cα RMSF as a function of residue number. As expected, the largest fluctuations are for the loop between the two α-helices forming the hairpin and for two loops in the β-barrel domain. Interestingly, the first two (i.e., the hairpin and one of the two β-domain loops) appear to be correlated in their motion, as highlighted by the correlation matrix in Fig. 7 *B*. In particular, a correlation between the motion of residue 106 at the tip of the helical hairpin and residue 213 in the β-barrel is observed.

DISCUSSION

Although the mechanism of drug extrusion used by Gram-negative bacteria remains incompletely characterized, the coparticipation of an IM protein and on OM protein is generally accepted. It is also established that these two proteins interact via a third periplasmic protein. In this work we analyzed the results of three extended simulations of the dynamics of one of those 'accessory' proteins, MexA from *P. aeruginosa*. The results of these MD simulations provide us with an insight into the dynamic behavior of the protein.

We observed a relatively flexible behavior, although the protein fold remained stable during the whole 20–25 ns of each simulation. The major motions correspond to interdomain motions, rather than flexibility within a given domain. The observed interdomain motions are the result of two principal motions. These latter consist of a bending of the protein involving the two principal domains, the helical hairpin and the β-strands, and a rotation of one domain with respect to the other (Fig. 4). It is of interest to note that site-directed spin labeling studies of AcrA have indicated pH-induced conformational changes (35).

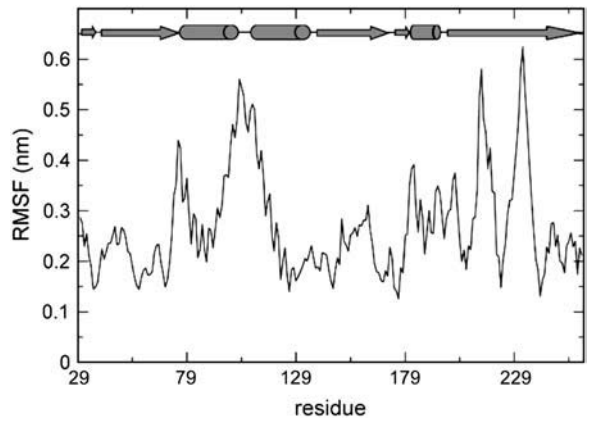

FIGURE 6 RMSF of Cα atoms with respect to their average position over the 25-ns simulation (MD1). A cartoon representation of the topology of the protein is shown above the graph.

Thus, PCA reveals two motions that provide an element of flexibility, which is likely to be exploited in the adaptor function of MexA. In the x-ray structures of both TolC and OprM, the lower (i.e., periplasmic) part of the protein is formed by an α-helical domain. In this domain, the helices twist in a coiled coil conformation. This region of the OM protein could interact with the helical hairpin of the periplasmic protein. Additionally, the β-strands of MexA could interact with the upper part of the IM protein, the so-called docking domain. Some rearrangements of MexA may be needed to enable it to interact with the IM and the OM proteins (20). It is possible that such interactions may modulate the intrinsic pattern of flexibility of the MexA molecule. Thus, MexA could adopt a different angle between the domains, as indicated by the first principal motion, or a different orientation of the two domains with respect to one another, as shown by the second eigenvector. A further possibility is that a concerted motion, which includes both the eigenvectors observed in the MD simulations, plays a functionally important role.

It thus seems likely that the flexibility of MexA is an important, and probably essential, requirement for this periplasmic protein to act as an adaptor between the two membrane proteins. This adaptor activity of MexA is necessary to allow the formation of a long channel able to span the whole periplasmic region and to extrude the drugs from inside the cell to the outside. In our simulations, we observed the protein to sample two different conformations while passing through the x-ray structure. This might lead us to hypothesize either an energy profile with two minima and one saddle point (the x-ray structure) or one with three minima. The latter hypothesis is perhaps in better agreement with stability of the conformation adopted by the protein during the crystallization process. We do not exclude the existence of other minima, probably reached by the protein after interaction with the IM or the OM protein. The timescale of the latter process is still beyond the limit of atomistic simulations.

In the crystal structures of AcrB and TolC the pore running through the center of each protein is closed (at the periplasmic mouth of the pore in the case of TolC and OprM). It is possible that the interaction between TolC/OprM and the adaptor protein (i.e., AcrA/MexA) leads to opening of the pore. In the proposed mechanism of opening of the OM protein (8,36) a twisting of the helices, involving especially the lower part of the protein, is required. This may be related to the rotation and twisting of the α-helical hairpin of the periplasmic protein, revealed by the first eigenvector. The enlargement and closing of the angle between the two main domains, corresponding to the second eigenvector, could be involved in the interaction of MexA with both the inner and the OM proteins. We therefore suggest a mechanism in which MexA aids the opening of the OM protein, with a rotation of its helical domain (first eigenvector), after close interaction with the helical domain of the latter. MexA

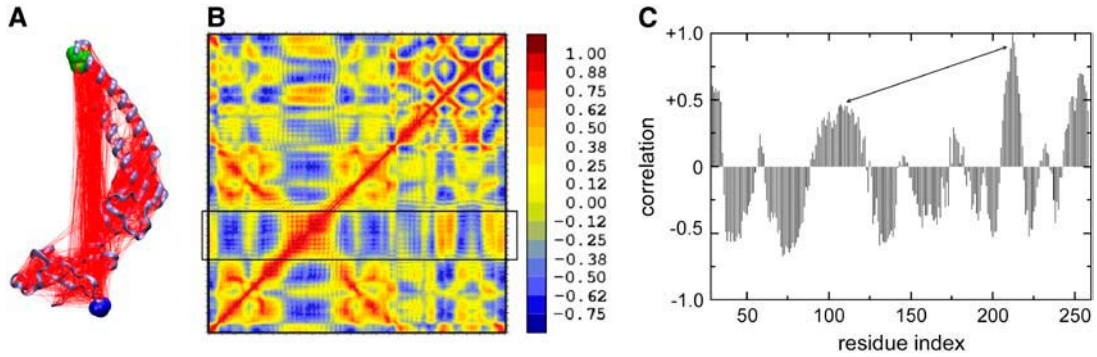

FIGURE 7 Correlated motions in simulation MD1. (*A*) Motions with 50% correlation are indicated by lines connecting the correlated residues. Residues 106 and 213 are highlighted in green and blue, respectively. (*B*) Correlation matrix obtained by the covariance matrix; results are normalized and a gradient of colors from red (positive correlation) to blue (negative) is used. The results are normalized so that the extreme values of 1 and −1 correspond to complete correlation of motion at all the time, along the same direction, and along opposite directions, respectively. The box indicates the correlation for the α-helical hairpin. (*C*) Correlation of residue 213 (the *blue sphere* in *A*, located in the β-barrel domain) with the whole protein. The arrow indicates a positive correlation between this residue and the tip of the α-helical hairpin (residue 106).

would also 'clamp' together IM and OM proteins with a flexible change in the angle between its two main domains (second eigenvector). Current models of the assembled transporter complex place the helical hairpin (around 101) in contact with the OM component and the correlated region around 213 close to the IM component. One might speculate that the observed MexA 106–213 correlated motion could link corresponding movements of the IM and OM components, and thus could be central to the opening mechanism.

Since the submission of this work, the structure of AcrA has been determined (14). The fold of AcrA is, as expected, very similar to that of MexA. Interestingly, comparison of the four AcrA monomer structures in the asymmetric unit of the AcrA crystal structure reveals significant differences in their conformation. In particular, the four x-ray structures suggest hinge bending at the junction between the helix hairpin and lipoyl domains. The maximum difference in hinge angle the authors observe is ~15°. If we calculate the equivalent angle for simulation MD1 of MexA, using the lipoyl subdomain as a reference and the vector from the base to the tip of the α-helical hairpin, the range is 19°. Thus, the x-ray structure of AcrA and the simulations of MexA seem to point toward a comparable degree of flexibility in these two homologs. This strongly supports our suggestion of dynamic flexibility in the MexA molecule.

Of course, simulation studies are a complement to experimental studies, and we should remain aware of the potential limitations of both approaches. In the case of the simulations, their duration is such as to result in incomplete sampling of conformational space (37). However, we note that three simulations (with similar starting conditions but different initial velocities) yielded a similar picture of the interdomain dynamics of MexA, and so we are reasonably confident of the robustness of the result presented in this work. Furthermore, the simulations described are of the monomeric form of MexA, and it is possible that the conformational dynamics are modulated when a protein/protein complex is formed (38). However, simulations of the monomer do reveal its intrinsic flexibility and so aid in the process of forming a more complete picture of the mechanism of the tripartite drug transport complex. This provides a specific example of a more general role for extended MD simulations as a method for unmasking the interdomain dynamics of components of multi-protein assemblies.

We thank Alessandro Grottesi for his interest and comments.

This work was funded by grants from the Wellcome Trust.

REFERENCES

1. Lewis, K. 1994. Multidrug resistance pumps in bacteria: variations on a theme. *Trends Biochem. Sci.* 19:119–123.
2. Nikaido, H. 1996. Multidrug efflux pumps of Gram-negative bacteria. *J. Bacteriol.* 178:5853–5859.
3. Poole, K., K. Krebes, C. McNally, and S. Neshat. 1993. Multiple antibiotic resistance in *Pseudomonas aeruginosa*: evidence for involvement of an efflux operon. *J. Bacteriol.* 175:7363–7372.
4. Fralick, J. A. 1996. Evidence that TolC is required for functioning of the mar/acrab efflux pump of *Escherichia coli*. *J. Bacteriol.* 178:5803–5805.
5. Buchanan, S. K. 2001. Type I secretion and multidrug efflux: transport through the TolC channel-tunnel. *Trends Biochem. Sci.* 26:3–6.
6. Koronakis, V., J. Eswaran, and C. Hughes. 2004. Structure and function of TolC: the bacterial exit duct for proteins and drugs. *Annu. Rev. Biochem.* 73:467–489.
7. Eswaran, J., E. Koronakis, M. K. Higgins, C. Hughes, and V. Koronakis. 2004. Three's company: component structures bring a closer view of tripartite drug efflux pumps. *Curr. Opin. Struct. Biol.* 14:717–747.
8. Koronakis, V., A. Sharff, E. Koronakis, B. Luisi, and C. Hughes. 2000. Crystal structure of the bacterial membrane protein TolC central to multidrug efflux and protein export. *Nature*. 405:914–919.
9. Murakami, S., R. Nakashima, E. Yamashita, and A. Yamaguchi. 2002. Crystal structure of bacterial multidrug efflux transporter AcrB. *Nature*. 419:587–593.

10. Akama, H., M. Kanemaki, T. Tsukihara, A. Nakagawa, and T. Nakae. 2004. Crystal structure of the drug discharge outer membrane protein, OprM, of *Pseudomonas aeruginosa*: dual modes of membrane anchoring and occluded cavity end. *J. Biol. Chem.* 279:52816–52819.

11. Federici, L., D. Du, F. Walas, H. Matsumura, J. Fernandez-Recio, K. S. McKeegan, M. I. Borges-Walmsley, B. F. Luisi, and A. R. Walmsley. 2005. The crystal structure of the outer membrane protein VceC from the bacterial pathogen *Vibrio cholerae* at 1.8 Å resolution. *J. Biol. Chem.* 280:15307–15314.

12. Higgins, M. K., E. Bokma, E. Koronakis, C. Hughes, and V. Koronakis. 2004. The structure of the periplasmic component of a drug efflux pump. *Proc. Natl. Acad. Sci. USA.* 101:9994–9999.

13. Akama, H., T. Matsuura, S. Kashiwagi, H. Yoneyama, T. Tsukihara, A. Nakagawa, and T. Nakae. 2004. Crystal structure of the membrane fusion protein, MexA, of the multidrug transporter in *Pseudomonas aeruginosa*. *J. Biol. Chem.* 279:25939–25942.

14. Mikolosko, J., K. Bobyk, H. I. Zgurskaya, and P. Ghosh. 2006. Conformational flexibility in the multidrug efflux system protein AcrA. *Structure.* 14:577–587.

15. Johnson, J. M., and G. M. Church. 1999. Alignment and structure prediction of divergent protein families: periplasmic and outer membrane proteins of bacterial efflux pumps. *J. Mol. Biol.* 287:695–715.

16. Zgurskaya, H. I., and H. Nikaido. 1999. AcrA is a highly asymmetric protein capable of spanning the periplasm. *J. Mol. Biol.* 285:409–420.

17. Touzé, T., J. Eswaran, E. Bokma, E. Koronakis, C. Hughes, and V. Koronakis. 2004. Interactions underlying assembly of the Escherichia coli AcrAB-TolC multidrug efflux system. *Mol. Microbiol.* 53:697–706.

18. Elkins, C. A., and H. Nikaido. 2003. Chimeric analysis of AcrA function reveals the importance of its C-terminal domain in its interaction with the AcrB multidrug efflux pump. *J. Bacteriol.* 185:5349–5356.

19. Nehme, D., X. Li, R. Elliot, and K. Poole. 2004. Assembly of the MexAB-OprM multidrug efflux system of *Pseudomonas aeruginosa*: identification and characterization of mutations in MexA compromising MexA multimerization and interaction with MexB. *J. Bacteriol.* 186:2973–2983.

20. Fernandez-Recio, J., F. Walas, L. Federici, J. Venkatesh Patrap, V. N. Bavro, R. Nunez Miguel, K. Mizuguchi, and B. Luisi. 2004. A model of a transmembrane drug-efflux pump from Gram-negative bacteria. *FEBS Lett.* 578:5–9.

21. Karplus, M. J., and J. A. McCammon. 2002. Molecular dynamics simulations of biomolecules. *Nat. Struct. Biol.* 9:646–652.

22. Krebs, W. G., V. Alexandrov, C. A. Wilson, N. Echols, H. Yu, and M. Gerstein. 2002. Normal mode analysis of macromolecular motions in a database framework. *Proteins.* 48:682–695.

23. Vriend, G. 1990. WhatIf—a molecular modeling and drug design program. *J. Mol. Graph.* 8:52–56.

24. Lindahl, E., B. Hess, and D. van der Spoel. 2001. GROMACS 3.0: a package for molecular simulation and trajectory analysis. *J. Mol. Model. (Online).* 7:306–317.

25. Hess, B., H. Bekker, H. J. C. Berendsen, and J. G. E. M. Fraaije. 1997. LINCS: a linear constraint solver for molecular simulations. *J. Comput. Chem.* 18:1463–1472.

26. Darden, T., D. York, and L. Pedersen. 1993. Particle mesh Ewald—an N.log(N) method for Ewald sums in large systems. *J. Chem. Phys.* 98:10089–10092.

27. Essmann, U., L. Perera, M. L. Berkowitz, T. Darden, H. Lee, and L. G. Pedersen. 1995. A smooth particle mesh Ewald method. *J. Chem. Phys.* 103:8577–8593.

28. Berendsen, H. J. C., J. P. M. Postma, W. F. van Gunsteren, A. DiNola, and J. R. Haak. 1984. Molecular dynamics with coupling to an external bath. *J. Chem. Phys.* 81:3684–3690.

29. Kabsch, W., and C. Sander. 1983. Dictionary of protein secondary structure: pattern-recognition of hydrogen-bonded and geometrical features. *Biopolymers.* 22:2577–2637.

30. Barrett, C. P., B. A. Hall, and M. E. M. Noble. 2004. Dynamite: a simple way to gain insight into protein motions. *Acta Crystallogr. D.* 60:2280–2287.

31. Humphrey, W., A. Dalke, and K. Schulten. 1996. VMD—visual molecular dynamics. *J. Mol. Graph.* 14:33–38.

32. Amadei, A., A. B. M. Linssen, and H. J. C. Berendsen. 1993. Essential dynamics of proteins. *Proteins.* 17:412–425.

33. Garcia, A. E. 1992. Large-amplitude nonlinear motions in proteins. *Phys. Rev. Lett.* 68:2696–2699.

34. Tai, K., T. Shen, U. Börjesson, M. Philippopoulos, and J. A. McCammon. 2001. Analysis of a 10-ns molecular dynamics simulation of mouse acetylcholinesterase. *Biophys. J.* 81:715–724.

35. Ip, H., K. Stratton, H. Zgurskaya, and J. Liu. 2003. pH-induced conformational changes of AcrA, the membrane fusion protein of Escherichia coli multidrug efflux system. *J. Biol. Chem.* 278:50474–50482.

36. Andersen, C., E. Koronakis, E. Bokma, J. Eswaran, D. Humphreys, C. Hughes, and V. Koronakis. 2002. Transition to the open state of the TolC periplasmic tunnel entrance. *Proc. Natl. Acad. Sci. USA.* 99:11103–11108.

37. Faraldo-Gómez, J. D., L. R. Forrest, M. Baaden, P. J. Bond, C. Domene, G. Patargias, J. Cuthbertson, and M. S. P. Sansom. 2004. Conformational sampling and dynamics of membrane proteins from 10-nanosecond computer simulations. *Proteins.* 57:783–791.

38. Goh, C. S., D. Milburn, and M. Gerstein. 2004. Conformational changes associated with protein-protein interactions. *Curr. Opin. Struct. Biol.* 14:104–109.